Chapter VI

CHAPTER VI

METAL-ORGANIC FRAMEWORK OF STRONTIUM-1-NAPHTHOATE: SYNTHESIS AND ITS CHARACTERIZATION

6.1 INTRODUCTION

Metal-organic frameworks (MOFs) are organic-inorganic hybrid materials with crystalline pores that are made up of an expected arrangement of positively charged metal ions encircled by organic "linker" molecules. The metal ions act as nodes, connecting the linkers' arms to create a repeating, cage-like structure. The internal surface area of MOFs is incredibly vast because of their hollow structure [1]. The present study dealt with the synthesis of MOF-Sr a novel type of crystal. Furthermore, in carboxylic acid, the hydrogen atom performs as an electron acceptor and the oxygen atom acts as an electron donor by making hydrogen bonds through supramolecular interaction to obtain MOF-Sr in a single crystal [2]. They were characterized by single-crystal XRD, FT-IR spectroscopy, and TG-DTA. The molecular structure was also analyzed using density functional theory (DFT), which closely resembles the single crystal analysis. Hirshfeld surface and 2D fingerprints provide detailed insight into various weak forces in molecular packing. The outcome of the result is discussed in Chapter 6.

6.2 EXPERIMENT

6.2.1 Preparation of MOF crystal growth

1 mmol of strontium (II) nitrate and 2 mmol of naphthoic acid were dissolved in 5 ml of a solution containing 2 ml of methanol, and 3 ml of water was gradually added under stirring. Then, the above solution was refluxed for 6 hours, filtered, and kept at room temperature without disturbing for 25 days. White solid crystals were obtained and washed with acetone/water to remove impurities, which are examined in **Figure 6.1** [3].

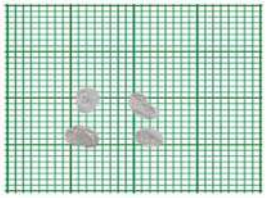

Figure 6.1 *Image of Crystal*

6.3 RESULT AND DISCUSSION

6.3.1 MOF-Crystal structure

The MOF-Sr crystal structure is shown in **Figure 6.2 a**. The space group of the crystal is monoclinic and possesses C2/c symmetry. The crystallographic data are exposed in **Table 6.1**. The bond angle and parameter were discussed in **Tables 6.2 and 6.3**. **Figure 6.2 b** represents the ORTEP crystal packing, and the formula obtained is $C_{22}H_{18}O_6Sr$. The acid and the metals are linked through the oxygen, and they are represented by Sr…. O, and the **Figure 6.2 c** crystal shows the short contacts of VdW radii of intermolecular. As a result, the crystal is viewed along the a, b, and c axes, and they are obtained as a slipped stacking arrangement, and the space-filling model represents the graphical presentation of geometrical relationships, which are shown in **Figure 6.3 (a-e)** [4]**.**

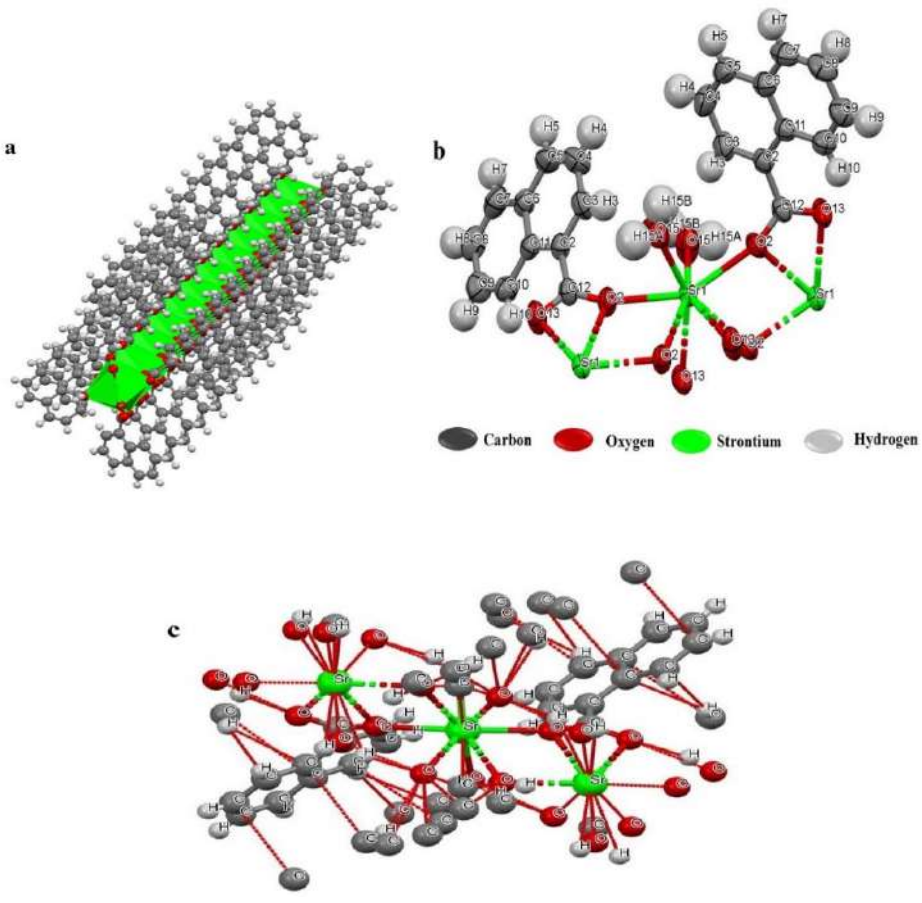

Figure 6.2 *a) MOF-Sr (b) Molecular ORTEP diagram (c) Short contacts*

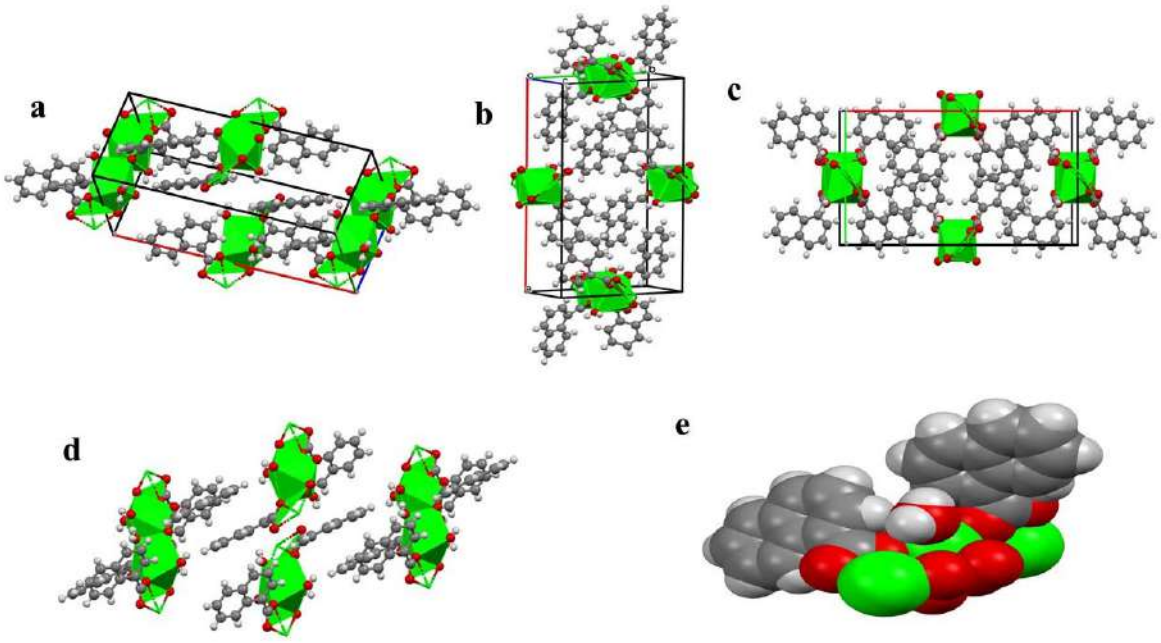

Figure 6.3 *Crystal observed along (a) 'a' axis direction, (b) 'b' axis direction, (c) 'c' axis direction, (d) Slipped stacking arrangement, and e) space-filling model.*

Table 6.1 *Crystallographic data and parameters of MOF-Sr*	
Empirical formula	$C_{22}H_{18}O_6Sr$
Temperature	(283-303) K
Crystal structure	Monoclinic
Space group	C2/c
Cell lengths (Å)	**a** 21.3817(3) **b** 11.4254(2) **c** 7.95460(10)
Cell angles (°)	**α** 90 **β** 93.9360(10) **γ** 90
Cell Volume ($Å^3$)	1938.68
Z, Z'	**Z**: 4 **Z'**: 0
Absorption coefficient (mm^{-1})	0.708782
R- factor (%)	2.03

Table 6.2 *Bond length of MOF-Sr.*

Atom1	Atom2	Cyclicity	Length
Sr1	O2	cyclic	2.491
O2	Sr1	cyclic	2.491
Sr1	O15	acyclic	2.584
O15	Sr1	acyclic	2.584
Sr1	O2	cyclic	2.491
O2	Sr1	cyclic	2.491
Sr1	O15	acyclic	2.584
O15	Sr1	acyclic	2.584
Sr1	O2	cyclic	2.689
O2	Sr1	cyclic	2.689
Sr1	O2	cyclic	2.689
O2	Sr1	cyclic	2.689
Sr1	O13	acyclic	2.623
O13	Sr1	acyclic	2.623
Sr1	O13	acyclic	2.623
O13	Sr1	acyclic	2.623
O2	C12	cyclic	1.259(2)
C12	O2	cyclic	1.259(2)
O2	Sr1	cyclic	2.689
Sr1	O2	cyclic	2.689
O13	C12	cyclic	1.255(2)
C12	O13	cyclic	1.255(2)
O13	Sr1	cyclic	2.623
Sr1	O13	cyclic	2.623
O15	H15A	acyclic	0.85(2)
H15A	O15	acyclic	0.85(2)
O15	H15B	acyclic	0.77(2)
H15B	O15	acyclic	0.77(2)
C11	C2	cyclic	1.430(2)
C2	C11	cyclic	1.430(2)
C11	C10	cyclic	1.415(2)
C10	C11	cyclic	1.415(2)

Atom1	Atom2	Cyclicity	Length
C11	C6	cyclic	1.421(2)
C6	C11	cyclic	1.421(2)
C2	C3	cyclic	1.373(3)
C3	C2	cyclic	1.373(3)
C2	C12	acyclic	1.504(3)
C12	C2	acyclic	1.504(3)
C3	H3	acyclic	0.93
H3	C3	acyclic	0.93
C3	C4	cyclic	1.408(3)
C4	C3	cyclic	1.408(3)
C10	H10	acyclic	0.93
H10	C10	acyclic	0.93
C10	C9	cyclic	1.369(3)
C9	C10	cyclic	1.369(3)
C6	C7	cyclic	1.420(3)
C7	C6	cyclic	1.420(3)
C6	C5	cyclic	1.414(3)
C5	C6	cyclic	1.414(3)
C9	H9	acyclic	0.93
H9	C9	acyclic	0.93
C9	C8	cyclic	1.407(3)
C8	C9	cyclic	1.407(3)
C7	H7	acyclic	0.93
H7	C7	acyclic	0.93
C7	C8	cyclic	1.352(3)
C8	C7	cyclic	1.352(3)
C5	H5	acyclic	0.93
H5	C5	acyclic	0.93
C5	C4	cyclic	1.359(3)
C4	C5	cyclic	1.359(3)
C8	H8	acyclic	0.93
H8	C8	acyclic	0.93
C4	H4	acyclic	0.93
H4	C4	acyclic	0.93

Atom1	Atom2	Cyclicity	Length
O2	C12	cyclic	1.259(2)
C12	O2	cyclic	1.259(2)
O2	Sr1	cyclic	2.689
Sr1	O2	cyclic	2.689
O13	C12	cyclic	1.255(2)
C12	O13	cyclic	1.255(2)
O13	Sr1	cyclic	2.623
Sr1	O13	cyclic	2.623
O15	H15A	acyclic	0.85(2)
H15A	O15	acyclic	0.85(2)
O15	H15B	acyclic	0.77(2)
H15B	O15	acyclic	0.77(2)
C11	C2	cyclic	1.430(2)
C2	C11	cyclic	1.430(2)
C11	C10	cyclic	1.415(2)
C10	C11	cyclic	1.415(2)
C11	C6	cyclic	1.421(2)
C6	C11	cyclic	1.421(2)
C2	C3	cyclic	1.373(3)
C3	C2	cyclic	1.373(3)
C2	C12	acyclic	1.504(3)
C12	C2	acyclic	1.504(3)
C3	H3	acyclic	0.93
H3	C3	acyclic	0.93
C3	C4	cyclic	1.408(3)
C4	C3	cyclic	1.408(3)
C10	H10	acyclic	0.93
H10	C10	acyclic	0.93
C10	C9	cyclic	1.369(3)
C9	C10	cyclic	1.369(3)
C6	C7	cyclic	1.420(3)
C7	C6	cyclic	1.420(3)
C6	C5	cyclic	1.414(3)
C5	C6	cyclic	1.414(3)

Atom1	Atom2	Cyclicity	Length
C9	H9	acyclic	0.93
H9	C9	acyclic	0.93
C9	C8	cyclic	1.407(3)
C8	C9	cyclic	1.407(3)
C7	H7	acyclic	0.93
H7	C7	acyclic	0.93
C7	C8	cyclic	1.352(3)
C8	C7	cyclic	1.352(3)
C5	H5	acyclic	0.93
H5	C5	acyclic	0.93
C5	C4	cyclic	1.359(3)
C4	C5	cyclic	1.359(3)
C8	H8	acyclic	0.93
H8	C8	acyclic	0.93
C4	H4	acyclic	0.93
H4	C4	acyclic	0.93
Sr1	O2	cyclic	2.491
O2	Sr1	cyclic	2.491
Sr1	O2	cyclic	2.491
O2	Sr1	cyclic	2.491

Table 6.3 *Bond angle of MOF-Sr.*

Atom1	Atom2	Cyclicity	Length
Sr1	O2	cyclic	2.491
O2	Sr1	cyclic	2.491
Sr1	O15	acyclic	2.584
O15	Sr1	acyclic	2.584
Sr1	O2	cyclic	2.491
O2	Sr1	cyclic	2.491
Sr1	O15	acyclic	2.584
O15	Sr1	acyclic	2.584
Sr1	O2	cyclic	2.689
O2	Sr1	cyclic	2.689
Sr1	O2	cyclic	2.689
O2	Sr1	cyclic	2.689
Sr1	O13	acyclic	2.623
O13	Sr1	acyclic	2.623
Sr1	O13	acyclic	2.623
O13	Sr1	acyclic	2.623
O2	C12	cyclic	1.259(2)
C12	O2	cyclic	1.259(2)
O2	Sr1	cyclic	2.689
Sr1	O2	cyclic	2.689
O13	C12	cyclic	1.255(2)
C12	O13	cyclic	1.255(2)
O13	Sr1	cyclic	2.623
Sr1	O13	cyclic	2.623
O15	H15A	acyclic	0.85(2)
H15A	O15	acyclic	0.85(2)

Atom1	Atom2	Cyclicity	Length
O15	H15B	acyclic	0.77(2)
H15B	O15	acyclic	0.77(2)
C11	C2	cyclic	1.430(2)
C2	C11	cyclic	1.430(2)
C11	C10	cyclic	1.415(2)
C10	C11	cyclic	1.415(2)
C11	C6	cyclic	1.421(2)
C6	C11	cyclic	1.421(2)
C2	C3	cyclic	1.373(3)
C3	C2	cyclic	1.373(3)
C2	C12	acyclic	1.504(3)
C12	C2	acyclic	1.504(3)
C3	H3	acyclic	0.93
H3	C3	acyclic	0.93
C3	C4	cyclic	1.408(3)
C4	C3	cyclic	1.408(3)
C10	H10	acyclic	0.93
H10	C10	acyclic	0.93
C10	C9	cyclic	1.369(3)
C9	C10	cyclic	1.369(3)
C6	C7	cyclic	1.420(3)
C7	C6	cyclic	1.420(3)
C6	C5	cyclic	1.414(3)
C5	C6	cyclic	1.414(3)
C9	H9	acyclic	0.93
H9	C9	acyclic	0.93
C9	C8	cyclic	1.407(3)

Atom1	Atom2	Cyclicity	Length
C8	C9	cyclic	1.407(3)
C7	H7	acyclic	0.93
H7	C7	acyclic	0.93
C7	C8	cyclic	1.352(3)
C8	C7	cyclic	1.352(3)
C5	H5	acyclic	0.93
H5	C5	acyclic	0.93
C5	C4	cyclic	1.359(3)
C4	C5	cyclic	1.359(3)
C8	H8	acyclic	0.93
H8	C8	acyclic	0.93
C4	H4	acyclic	0.93
H4	C4	acyclic	0.93
O2	C12	cyclic	1.259(2)
C12	O2	cyclic	1.259(2)
O2	Sr1	cyclic	2.689
Sr1	O2	cyclic	2.689
O13	C12	cyclic	1.255(2)
C12	O13	cyclic	1.255(2)
O13	Sr1	cyclic	2.623
Sr1	O13	cyclic	2.623
O15	H15A	acyclic	0.85(2)
H15A	O15	acyclic	0.85(2)
O15	H15B	acyclic	0.77(2)
H15B	O15	acyclic	0.77(2)
C11	C2	cyclic	1.430(2)
C2	C11	cyclic	1.430(2)

Atom1	Atom2	Cyclicity	Length
C11	C10	cyclic	1.415(2)
C10	C11	cyclic	1.415(2)
C11	C6	cyclic	1.421(2)
C6	C11	cyclic	1.421(2)
C2	C3	cyclic	1.373(3)
C3	C2	cyclic	1.373(3)
C2	C12	acyclic	1.504(3)
C12	C2	acyclic	1.504(3)
C3	H3	acyclic	0.93
H3	C3	acyclic	0.93
C3	C4	cyclic	1.408(3)
C4	C3	cyclic	1.408(3)
C10	H10	acyclic	0.93
H10	C10	acyclic	0.93
C10	C9	cyclic	1.369(3)
C9	C10	cyclic	1.369(3)
C6	C7	cyclic	1.420(3)
C7	C6	cyclic	1.420(3)
C6	C5	cyclic	1.414(3)
C5	C6	cyclic	1.414(3)
C9	H9	acyclic	0.93
H9	C9	acyclic	0.93
C9	C8	cyclic	1.407(3)
C8	C9	cyclic	1.407(3)
C7	H7	acyclic	0.93
H7	C7	acyclic	0.93
C7	C8	cyclic	1.352(3)

Atom1	Atom2	Cyclicity	Length
C8	C7	cyclic	1.352(3)
C5	H5	acyclic	0.93
H5	C5	acyclic	0.93
C5	C4	cyclic	1.359(3)
C4	C5	cyclic	1.359(3)
C8	H8	acyclic	0.93
H8	C8	acyclic	0.93
C4	H4	acyclic	0.93
H4	C4	acyclic	0.93
Sr1	O2	cyclic	2.491
O2	Sr1	cyclic	2.491
Sr1	O2	cyclic	2.491
O2	Sr1	cyclic	2.491

6.3.2 *Theoretical Morphology Study*

The morphology of the MOF-Sr crystal is generated with the help of WinXmorph computer software and the morphology of the grown crystal. The 8 well-developed faces of MOF-Sr crystal are (0,0,1), (0,0,-1), (0,1,0), (0,-1,0), (1,0,0) (-1,0,0), (1,0,-1) and (-1,0,1) is presented in **Figure 6.4 a**. The plane was also intimated by stereographic projection, as represented in **Figure 6.4b**. The arrangement of the chromophore is indicated by the acute angle, which exhibits the plane 'a axis in **Figure 6.4c**. The plane group is vertical to its cation molecular units. The axis 'a' denotes a 52.85° angle. The CCDC received the crystallographic file with reference number 1989649 [5].

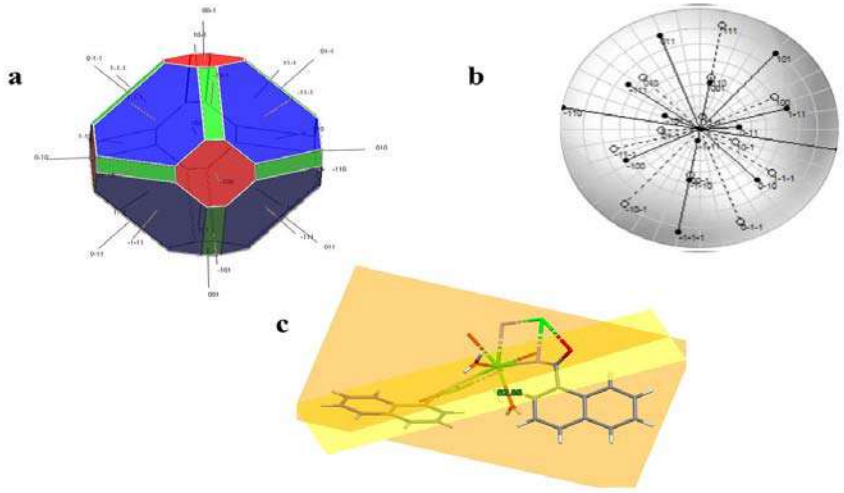

Figure 6.4 *(a) Morphology of MOF-Sr (b) Stereographic projection, (c) Acute angle along the plane 'a' axis.*

6.3.3 FT-IR spectra

The FTIR spectra of **Figure 6.5** show a peak at 3728-3031 cm^{-1} assigned for the H–O–H stretching vibrations. The peaks detected at 1686 cm^{-1} are due to the COOH group of naphthoic acid. The 1363 cm^{-1} is due to the C–O stretching vibration. The Sr-MOF peak appears at 690 cm^{-1}, which confirms the formation of the metal-organic framework and their stretching frequencies illustrated in **Table 6.4** [6].

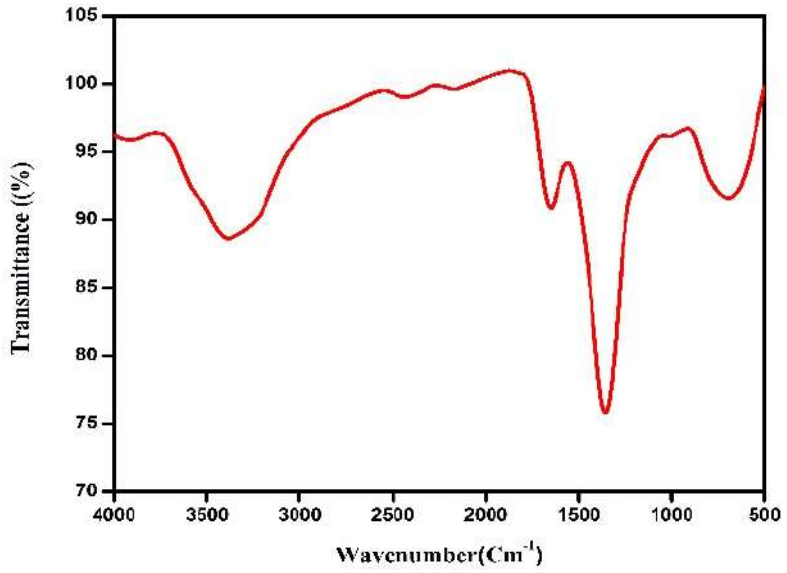

Figure 6.5 *FT-IR of MOF-Sr*

Table 6.4 *IR data of MOF-Sr*	
υ cm^{-1}	**Assignments**
690	ν_{M-O}
3354	ν_{OH}
1686	ν_{COO}
1337	C-O

6.3.4 UV-visible spectra

The optical properties of the MOF-Sr were illustrated in the UV-visible spectroscopy, which was recorded in the range of 200-800 nm. The peak at 290 nm is purely meant for MOF-Sr. The region where the optical cut-off wavelength is shown in **Figure 6.7a**.The absorption coefficient, Tauc's plot, refractive index, extinction coefficient, and skin depth were determined by UV-visible data. The absorption coefficient wavelength was determined by the equation **Eq.(6.1)**.

$$\alpha = \frac{2.303\ A}{t} \qquad \textbf{Eq.(6.1)}$$

The plot was drawn against the absorption coefficient vs. energy band (Eg) shown in **Figure 6.7b,** and the fundamental absorption was noticed at 4.0 eV. **Figure 6.7c** represented Tauc's plot, and the energy band gap was determined by $\alpha h\nu = A(h\nu\text{-}Eg)^2$ in which the Eg values is found to be 3.9 eV. This is due to the semi-conducting nature of the compounds. **Figure 6.7d** examines the refractive index, which was calculated by $n = \{(1/T) + (1/(T\text{-}1)\}^{1/2}$ in which the higher refractive indexes were detected at 210 nm. This is due to the effect of fundamental absorption. **Figure 6.7e** exhibits the extinction coefficient which was calculated using the equation $k = \alpha\lambda/4\pi$ and shows that the photon energy increases while the extinction coefficient increases, and then after 300 nm they are gradually reduced. **Figure 6.7f** determines the skin depth of the sample, which indicates that increasing the photon energy decreases the skin depth value [7].

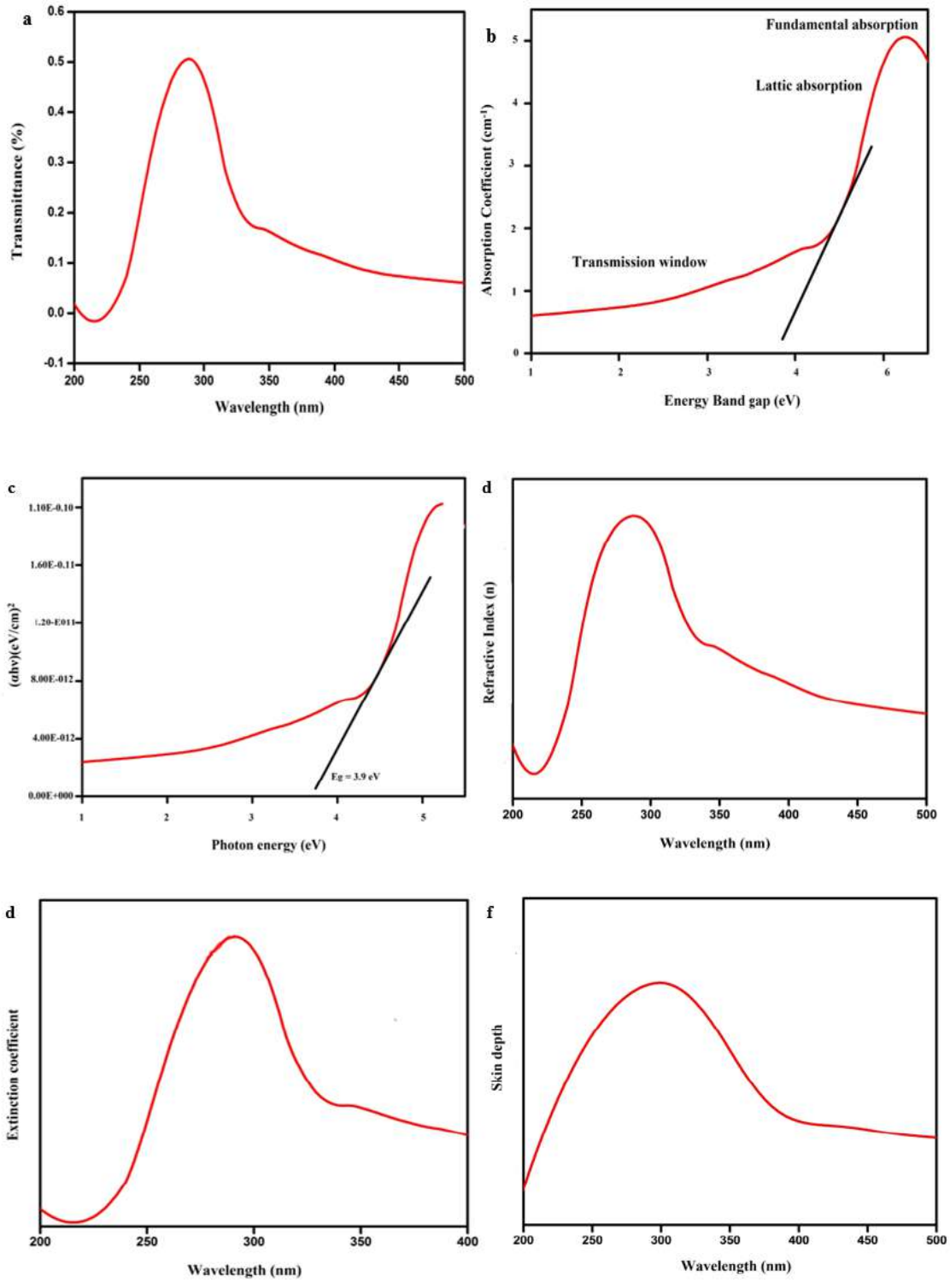

Figure 6.7 *(a) UV spectra of MOF-Sr, (b) Absorption coefficient, (c) Tauc's plot, (d) Refractive index, (e) Extinction coefficient, and (f) Skin Depth of the MOF-Sr.*

6.3.5 Thermal analysis

The thermal analysis of the MOF-Sr was performed from 100 to 600 °C at nitrogen atmospheric. **Figure 6.8** represents the stages of thermal decomposition. There is a slight decomposition at 55 °C due to the removal of the moisture in the compound. The first phase of decomposition at 250 °C encompassed the sharp endothermic peak, with the removal of water at this stage, and up to 300 °C, the crystal was stable. At last, a final decomposition occurred above 500°C, resulting in the formation of metal oxide as the final product. From this, it was evident that the crystal was thermally stable [7].

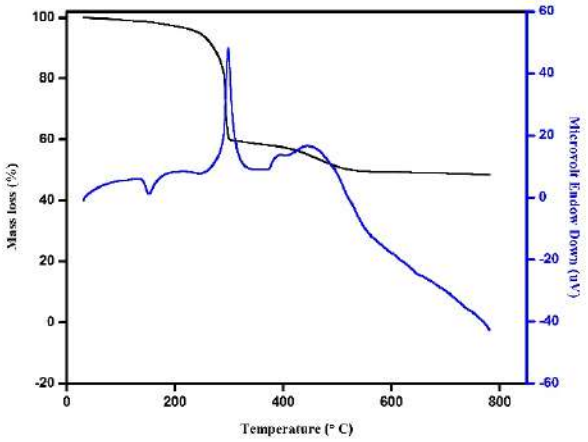

Figure 6.8 *Thermal Analysis of MOF-Sr*

Thermodynamic parameters were calculated using the Coats-Redfern equations,

$$\log_{10}\left[\frac{1-(1-\alpha)^{1-n}}{T^2\,(1-n)}\right] = \log_{10}\left[\frac{AR}{E\alpha}\right]\left[1-\frac{2RT}{E\alpha}\right] - \frac{E}{2.303\,RT} \qquad \textbf{Eq.(6.2)}$$

Where α, is the sample decomposed at a given time (t),

W_o is the initial weight,

W_f is the final weight,

W_t, the weight of the sample at any temperature.

T is an absolute temperature

A is the frequency factor

E is the activation energy and

R is gas constant

The plot was drawn against $\log_{10}\left[\frac{1-(1-\alpha)^{1-n}}{T^2\,(1-n)}\right]$ Vs **1/T** and is exposed in **Figure 6.9**, where three different stages of temperature decomposition take place at 543K, 693K, and 753K. The activation energies of E_a and slope values are tabulated in **Table 6.5**. The below formula is used to determine the enthalpy, entropy, and Gibbs free energy.

Entropy change, $\Delta S = R*\ln(Ah/kT)$ **Eq.(6.3)**

Enthalpy change, $\Delta H = E_a - RT$ **Eq.(6.4)**

Gibbs free energy $\Delta G = \Delta H - T\Delta S$ **Eq.(6.5)**

The negative value of ΔS represents that the reaction is slower, it gives more excellent reactants. The positive ΔH specifies the reaction occurs in the endothermic reaction, and the positive ΔG value proves they are non-spontaneous, in which 753 shows the slope values were correlated with the linear fit in which the R^2 value produced 0.99 [8].

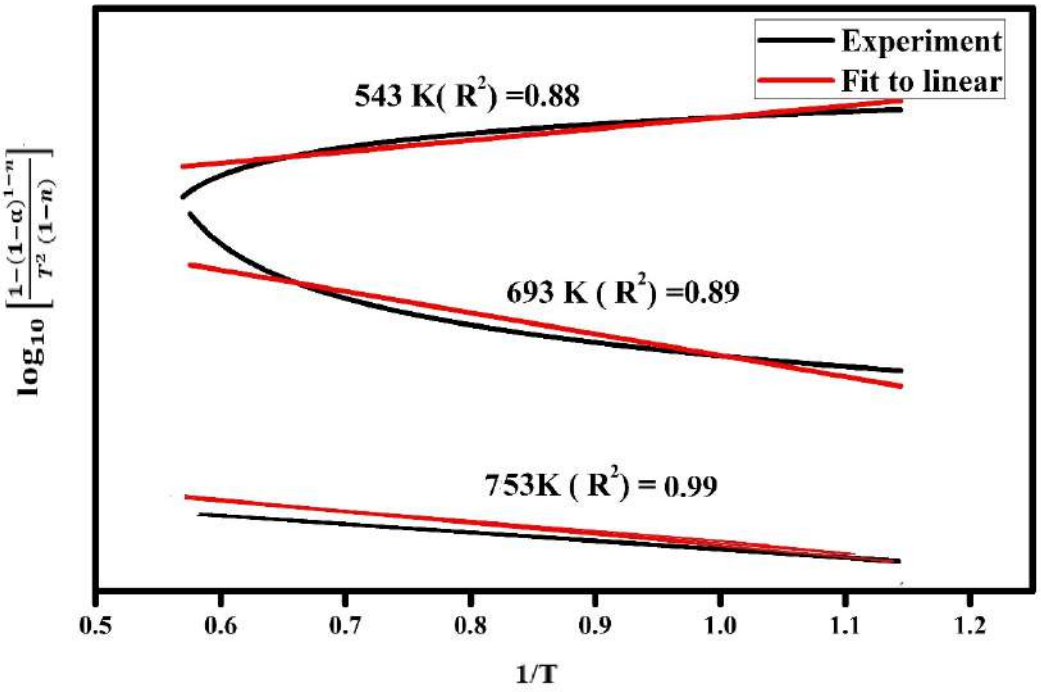

Figure 6.9 *Thermodynamic parameters (a) 543 K, (b) 793 K, and (c) 953 K.*

Table 6.5 *Thermodynamic parameters.*				
Temperature in K	**Ea kJ/mol**	**ΔS JK^{-1}/mol**	**ΔH kJ/mol**	**ΔG kJ/mol**
543	39.12	-22.41	26.43	13.08
693	39.12	-20.55	26.43	10.84
753	65.12	16.25	22.25	10.53

6.3.6 Powder- XRD

X-ray diffraction data for the MOF-Sr is shown in **Figure 6.10 (a)**. The values of d-spacing and intensity are related to determine isomorphism among the crystal. The peak diffraction was detected, and the hkl values were studied. It is evidenced by their composition and geometry, respectively which is compared with theoretical data illustrated in **Figure 6.10 (b)** [9].

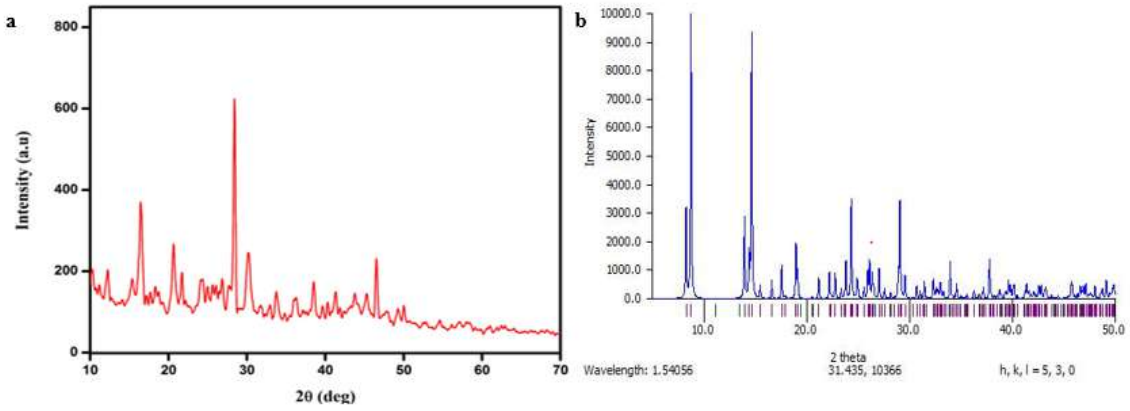

Figure 6.10 *Powdered-XRD (a)Experimental method (b) Theoretical method.*

6.4 COMPUTATIONAL STUDY FOR CRYSTAL

The atomic configuration of the ions was studied computationally using the Gaussian 09W software, and the stable geometry was obtained by optimizing using the DFT//B3LYP and their basic set with 6.31G(d,p) shown in **Figure 6.11a**.

Figure 6.11b determines the frontier molecular orbital, which signifies the chemical stability and interaction of the compounds on the active sites. The HOMO-LUMO suggests charge allocation among the aromatic ring and the nitro groups. The E_{HOMO} and E_{LUMO} values are -11.814 eV and -4.5054 eV, respectively. The negative values indicate the stability of the sample. The ΔE value is found to be 7.31 eV [10].

The global reactivity represents the chemical potential (μ), electro negativity (χ), chemical hardness (η), global softness (s), and electrophilicity (ω) which were calculated from HOMO and LUMO, where HOMO represents the ionization energy and LUMO describes the electron affinity of the crystal [9].

$$\mu = -(IE+EA) / 2 \qquad \textbf{Eq.(6.6)}$$

$$\chi = (IE+EA) / 2 \qquad \textbf{Eq.(6.7)}$$

$$\eta = (IE-EA) / 2 \qquad \textbf{Eq.(6.8)}$$

$$s = 1 / 2\eta \qquad \textbf{Eq.(6.9)}$$

$$\omega = \mu^2 / 2\eta \qquad \textbf{Eq.(6.10)}$$

The results of global reactivity are listed in **Table 6.6**. η and s indicate that Global softness (s) is less than chemical hardness (η) and electrophilicity (ω) shows a higher value, which signifies the charges from the closer molecules.

The Molecular Electrostatic Potential surface denotes the interaction of the molecule, electron density, electrophilicity, and nucleophilicity. **Figure 6.11c** describes the red, blue, and white colors. Negative electricity is signified by red, and positive electricity is denoted by blue. The range -0. 05 a.u, indicates the deep red color, to + 0.05 a. u represents the deep blue color. The surface is mostly covered in white, which indicates it is non-polar [11].

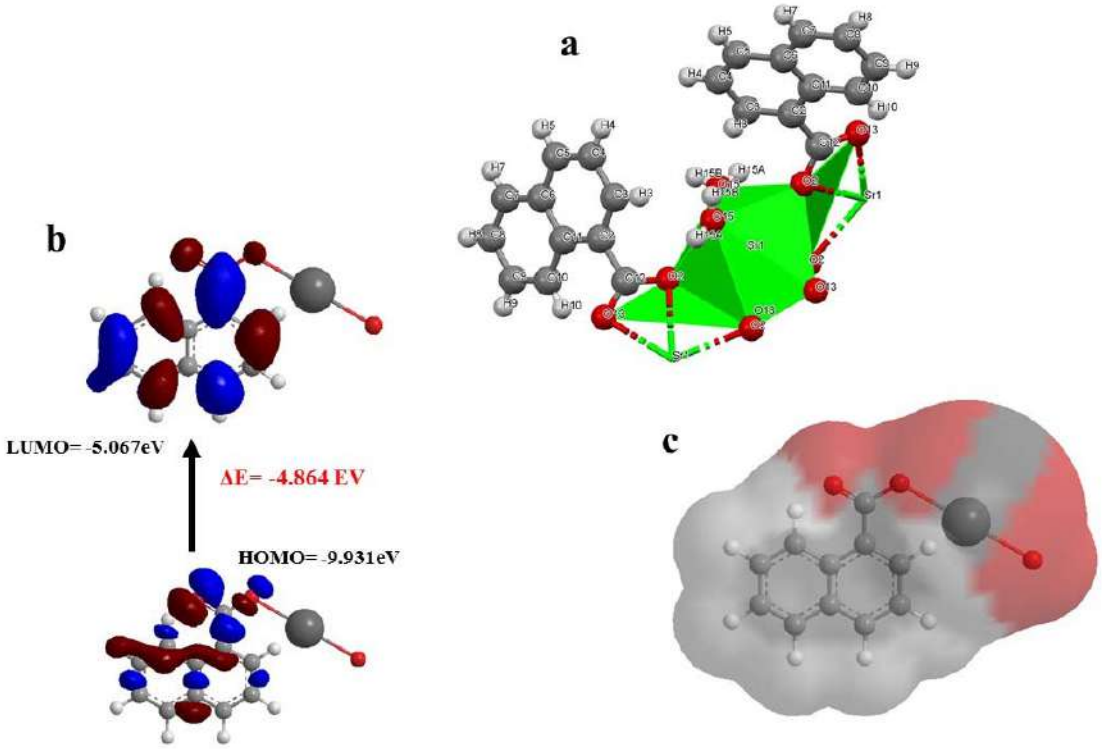

Figure 6.11 *(a) Geometrical orientation of MOF-Sr, (b) HOMO and LUMO of MOF-Sr, and (c) Molecular electrostatic potential of MOFs.*

Table 6.6 *Global reactivity descriptors value of MOFs.*	
Parameters	**Energy values (eV)**
Chemical potential (μ)	-16.318
Electronegativity (χ)	16.318
Chemical hardness (η)	3.655
Global softness (s)	1.8275
Electrophilicity (ω)	36.42

6.5 HIRSHFELD SURFACE ANALYSIS

Distances from the Hirshfeld surface to the nearest nucleus inside (internal d_i) and outside the surface (external, d_e) were the foremost functions of distance mapping which are shown in **Figure 6.12a**. It generates the $d_{norm,}$ in which two types of distance occur di (internal) and de (external), which ranges from -0.5727 (red) to 1.363 (blue). In a 3D image, the red region shows the oxygen, and atoms, and the hot spot is described as a hydrogen bond in contact with oxygen and nitrogen. **Figure 6.12b** describes the shape index, in which the mapping ranges from -1Å concave to convex for the crystal. This denotes the electron density between the compounds. The red region indicates the concave region, while the blue, the convex region. The Curved surface is examined in **Figure 6.12c,** in which several green flat areas are enclosed by light blue edges, which correspond to the low value of the curvedness. Fragment patches represent the different color patches that let us recognize the nearby compound in the same environment in **Figure 6.12d** [12].

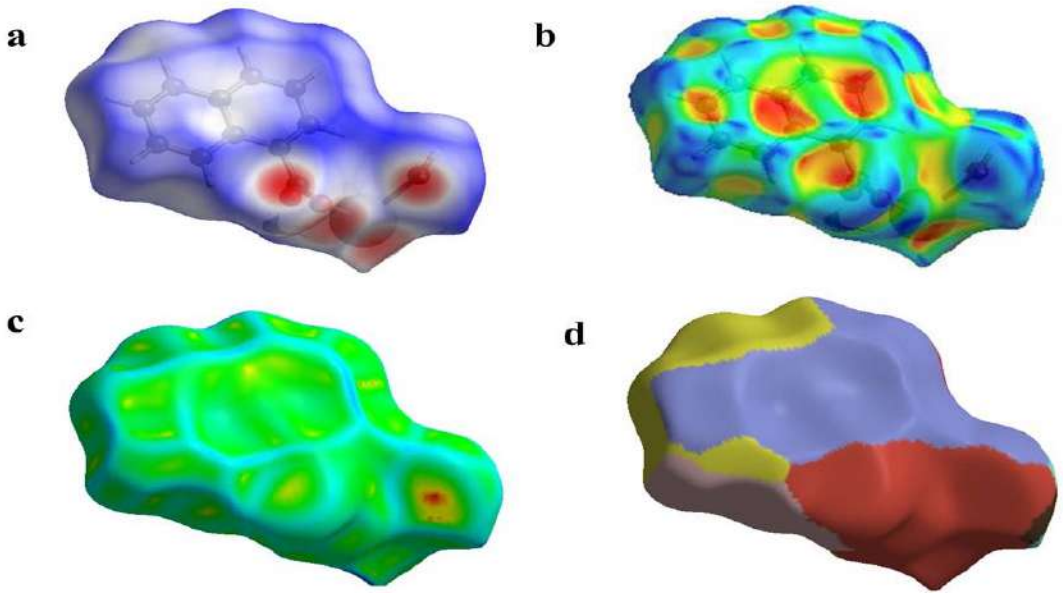

Figure 6.12 *Hirshfeld surface plots of the MOF-Sr (a) d_{norm}, (b) shape index, (c) curvedness, and (d) fragment patch.*

The 2D fingerprint plots of specific atomic interactions and overall interactions are shown in **Figure 6.13,** which signifies the intermolecular interaction between the molecules in the crystal pack as designated by their peaks exhibited in the plot. Individual

interactions in the crystal pack were H…O- 8.1%, C...O-1.1%, C…C-2.2%, O…O-9.3% and HO…C-O-0.8% , O…H-11.2 %, N…H-25.3 %, H…C-9.8 %, and C…H-13.2 % other interactions is weak.

The Hirshfeld surface in **Figure 6.14a** indicates the interaction of an atom inside MOF-Sr with all the neighborhood vicinity atoms in the crystal package Sr-All-12.9%, O-All-23.9 %, C-All-19.9 %, H-All-43.3%,. and **Figure 6.14b** represents the interaction of all the neighborhood atoms All-Sr-2.5 %, All-O-30.1%, All-C-16.2 %, All-H-51.1 %, The crystal packing for H-All shows their total interaction in compound [13].

Figure 6.15 displays the voids through the unit cell, which determine the mechanical strength of the compound. The volume is 196.92 $Å^3$ and the Area is 638.89 $Å^2$.

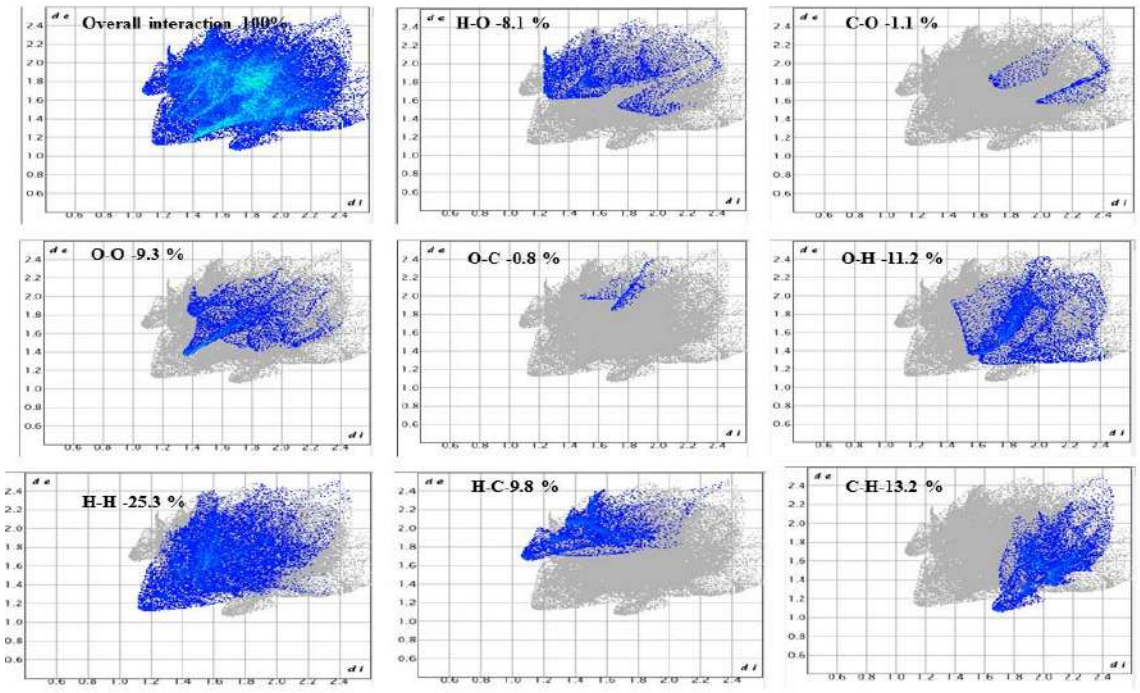

Figure 6.13 *2D fingerprint plots of individual atomic interactions and overall interactions.*

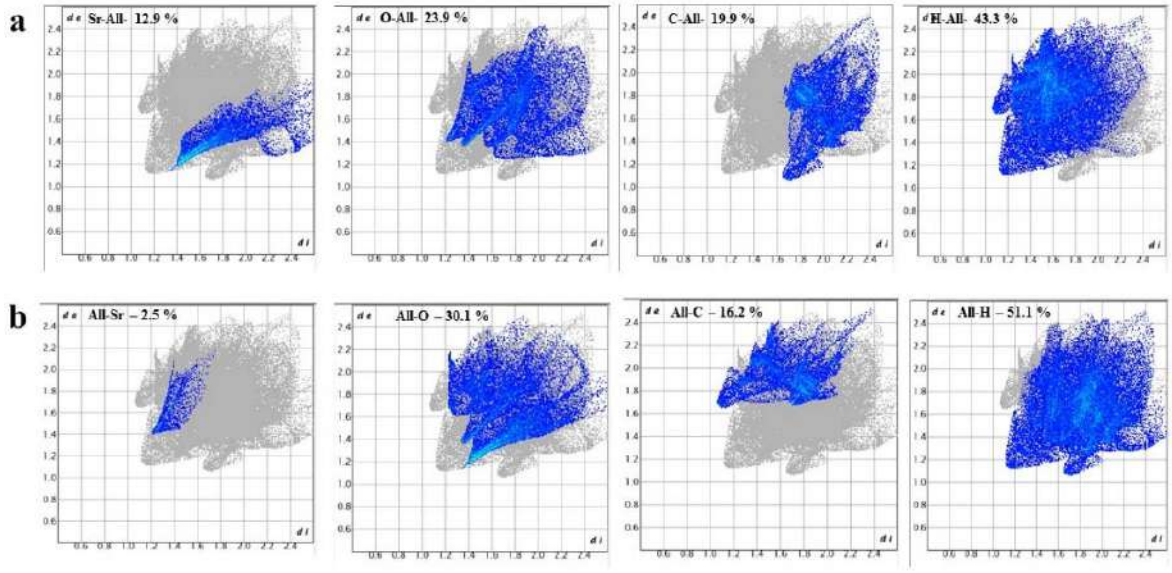

Figure 6.14 *Hirshfeld surface 2D fingerprint plots of (a) interactions of an atom inside a MOF with all the neighborhood vicinity atoms and (b) interactions of all the neighborhood atoms of the MOF with an atom in the crystal packing.*

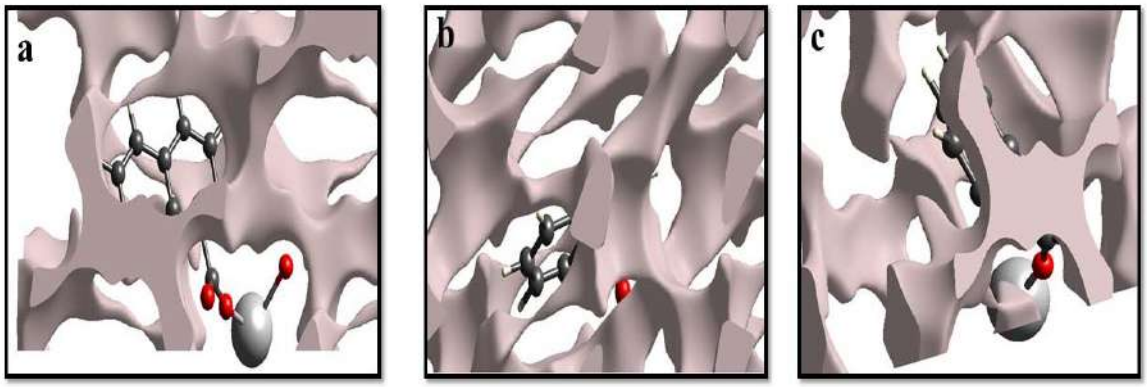

Figure 6.15 *Crystal voids of MOF projected along the a, b, and c axis.*

6.6 CONCLUSION

A novel metal-organic framework has been synthesized with 1-naphthoic acid and strontium in the form of a single crystal. The space group of the crystal is monoclinic, and it has C2/c symmetry. Theoretical crystal morphology exhibits eight sets of facets, and the distance between the planes is denoted by a 52.85° angle. In FTIR spectra, the peaks at 1686 cm^{-1} are due to the COOH group of naphthoic acid, Sr-MOF peak appears at 690 cm^{-1}

which conforms to the formation of a metal-organic framework. XRD data confirms the nature of MOFs is highly crystalline. The UV data represents the Eg value, which is calculated to be 3.9 eV, which confirms the semi-conducting nature. DFT and FMO demonstrate optimized geometry, energy gap (ΔE), chemical stability, and global reactivity descriptors. The Hirshfeld surface represented the 2D fingerprint plot, and crystal voids deliver data about the molecular interaction, electronic density, and intermolecular properties of close contacts.

REFERENCES

1. Wang, H., Zhu, Q. L., Zou, R. & Xu, Q. Metal-Organic Frameworks for Energy Applications. *Chem* **2**, 52–80 (2017).
2. Wang, B., Lin, R. B., Zhang, Z., Xiang, S. & Chen, B. Hydrogen-Bonded Organic Frameworks as a Tunable Platform for Functional Materials. *J. Am. Chem. Soc.* **142**, 14399–14416 (2020).
3. Ibrahim, A. A. *et al.* Applications of nanostructure phosphomolybdic acid/strontium MOF for removal of Rhodamine B and synthesis of pharmaceutically significant 14-Aryl-14-alkyl-14-H-dibenzoxanthene and 7-hydroxy-4-methyl coumarin. *Inorg. Chem. Commun.* **153**, 110748 (2023).
4. Y-y, J. *et al.* A Sr2-metalorganic framework with high chemical stability: synthesis, crystal structure and photoluminescence property. *Philos. Trans. R. Soc. A Math. Phys. Eng. Sci.* **375**, (2017).
5. Rohl, A. L. Computer prediction of crystal morphology. *Curr. Opin. Solid State Mater. Sci.* **7**, 21–26 (2003).
6. Ibrahim, A. A. *et al.* Green construction of eco-friendly phosphotungstic acid Sr-MOF catalysts for crystal violet removal and synthesis of coumarin and xanthene compounds. *RSC Adv.* **11**, 37276–37289 (2021).
7. Verma, A., Kumar, U., Chaudhary, P. & Yadav, B. C. Investigation on structural and optical properties of porous SnO2 nanomaterial fabricated by direct liquid injection chemical vapour deposition technique. *Solid State Commun.* **348**–**349**, 114723 (2022).
8. Takiishi, K. & Fujishiro, F. Determination of Thermodynamic Parameters for the Reaction between Perovskite-type BaFe1- xInxO3-δand CO2Using Thermogravimetry. *J. Phys. Chem. C* **126**, 20395–20400 (2022).
9. Wang, Y. *et al.* A novel tb@sr-mof as self-calibrating luminescent sensor for nutritional antioxidant. *Nanomaterials* **8**, (2018).

10. Raizada, M. *et al.* New hybrid polyoxovanadate-Cu complex with V···H interactions and dual aqueous-phase sensing properties for picric acid and Pd2+: X-ray analysis, magnetic and theoretical studies, and mechanistic insights into the hybrid's sensing capabilities. *J. Mater. Chem. C* **5**, 9315–9330 (2017).

11. Liu, L. *et al.* Molecular Electrostatic Potential: A New Tool to Predict the Lithiation Process of Organic Battery Materials. *J. Phys. Chem. Lett.* **9**, 3573–3579 (2018).

12. Ashfaq, M. *et al.* Synthesis, Crystal Structure, Hirshfeld Surface Analysis, and Computational Study of a Novel Organic Salt Obtained from Benzylamine and an Acidic Component. *ACS Omega* **6**, 22357–22366 (2021).

13. Sasikala, V., Kalyana Sundar, J. & Anna Lakshmi, M. Growth and physicochemical investigations on wide bandgap 2D polymeric amino acetic acid sulfato dilithium metal–organic framework. *J. Mater. Sci. Mater. Electron.* (2019).